

THE DARK DISK OF THE MILKY WAY

CHRIS W. PURCELL¹, JAMES S. BULLOCK¹, AND MANOJ KAPLINGHAT¹

Submitted to ApJ

ABSTRACT

Massive satellite accretions onto early galactic disks can lead to the deposition of dark matter in disk-like configurations that co-rotate with the galaxy. This phenomenon has potentially dramatic consequences for dark matter detection experiments. We utilize focused, high-resolution simulations of accretion events onto disks designed to be Galaxy analogues, and compare the resultant disks to the morphological and kinematic properties of the Milky Way's thick disk in order to bracket the range of co-rotating accreted dark matter. We find that the Milky Way's merger history must have been unusually quiescent compared to median Λ CDM expectations and therefore its dark disk must be relatively small: the fraction of accreted dark disk material near the Sun is about 20% of the host halo density or smaller and the co-rotating dark matter fraction near the Sun, defined as particles moving with a rotational velocity lag less than 50 km/s, is enhanced by about 30% or less compared to a standard halo model. Such a dark disk could contribute dominantly to the low energy (of order keV for a dark matter particle with mass 100 GeV) nuclear recoil event rate of direct detection experiments, but it will not change the likelihood of detection significantly. These dark disks provide testable predictions of weakly-interacting massive particle dark matter models and should be considered in detailed comparisons to experimental data. Our findings suggest that the dark disk of the Milky Way may provide a detectable signal for indirect detection experiments, contributing up to about 25% of the dark matter self-annihilation signal in the direction of the center of the Galaxy, lending the signal a noticeably oblate morphology.

Subject headings: Cosmology: theory — galaxies: formation — galaxies: evolution

1. INTRODUCTION

Prospects for the direct detection of dark matter depend crucially on the phase space distribution of dark matter near the Sun (Smith & Lewin 1990; Jungman et al. 1996; Vogelsberger et al. 2009). Unfortunately, detailed predictions for the dark matter distribution around the Earth are extremely difficult to construct from first principles; they require an understanding of spatial clumping on the scale of the Solar System (Kamionkowski & Koushiappas 2008; Peter 2009), and are almost certainly affected by poorly-understood baryonic processes like the formation of the Galactic disk.

Recently, Read et al. (2008, 2009) emphasized that the process of cosmological disk galaxy formation can significantly alter the dark matter distribution compared to canonical predictions that rely on simulations of the standard halo model. During the process of hierarchical structure formation, merging satellite galaxies can get dragged into the plane of their host disk and deposit their dark matter in a structure, dubbed the *dark disk* (Read et al. 2008), that is co-rotating with the Milky Way stellar disk and morphologically resembles a thick disk. If the Λ CDM cosmology represents the correct model of structure formation in the universe, it is certain that dark disks are virtually ubiquitous in disk galaxies. However, this contribution relative to the smoother halo component will depend sensitively on the formation process of each galaxy individually. In this work, we provide the first focused attempt at constraining the dark disk contribution in the Galaxy, improving upon the ini-

tial discussion of the Milky Way dark disk in Read et al. (2008) by comparing our simulations to the detailed kinematic and morphological properties of the Galactic thick disk.

If a substantial dark disk exists within the Milky Way, then it has dramatic implications for the direct and indirect detection of dark matter, should that species consist of Weakly Interacting Massive Particles (WIMPs), which are pervasive in models of new physics at the weak scale. A co-rotating disk of dark matter will leave temporal modulation signals in terrestrial nuclear-recoil experiments. It will also increase WIMP capture in the Sun and Earth and enhance the resultant flux of neutrinos from WIMP self-annihilation; both of these results have been discussed in detail by Bruch et al. (2009a,b). We show in this work that a disk-like structure could be discernible in the self-annihilation signal (depending on the total flux) from the center of the galaxy. Since the scale height of the dark matter disk will be larger than the thin disk scale height and smaller than any background halo flattening, such a morphological feature could provide an important handle on this indirect detection signal.

The fraction of dark matter locked up in a co-rotating component is expected to depend sensitively on merger history (Read et al. 2009), and this creates an important link between dark matter detection experiments and efforts in Galactic astronomy to constrain the accretion history of the Milky Way. Evidence is mounting that the merger history of the Galaxy is unusually quiescent compared to *typical* Λ CDM expectations (Wyse 2009). High-resolution simulations have shown that 1:10 mass-ratio accretion events, despite being fairly common in the Λ CDM paradigm (Stewart et al. 2008), are irreconcilable

Electronic address: cpurcell@uci.edu

¹ Center for Cosmology, Department of Physics and Astronomy, The University of California, Irvine, CA 92697 USA

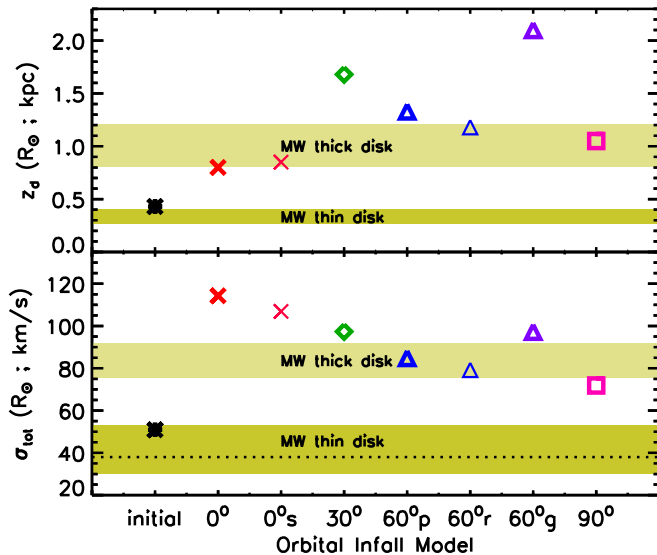


FIG. 1.— Morphological and dynamical properties of the final stellar disks at the solar neighborhood for each fiducial orbital infall condition: the disk scale height z_d in kpc (*upper panel*), and the total velocity dispersion σ_{tot} in km/s (*lower panel*). The shaded regions indicate observational boundaries: the Galactic scale heights and their errors are drawn from the SDSS tomographic results reported by Jurić et al. (2008), while the dynamical temperature ranges represent the thin-disk spread observed by Nordström et al. (2004) for total velocity dispersion as a function of stellar age in the solar neighborhood (the region represents stars with ages between 1 Gyr and 8 Gyr and the *dotted* line marks the velocity dispersion for stars with a median age of $\sim 2 - 3$ Gyr), and the thick-disk range corresponds to the dispersions reported by Soubiran et al. (2003). The infall model denoted by 0°_s represents the accretion event involving a slower satellite galaxy; the three 60° infall models are marked with prograde, retrograde, and gas, according to the methods outlined in §2 and as listed in Table 1.

with the cold and thin Galactic disk (Purcell et al. 2009a, hereafter PKB09). This conclusion is consistent with the results of Read et al. (2008) and Villalobos & Helmi (2008), who used simulations to show that 1:10 mergers generate heated systems that are grossly consistent galactic *thick disks*, but that are clearly incommensurable with the dominant thin disk of the Galaxy. More recently, the simulations of Moster et al. (2009) showed that while these common mergers may be consistent with the broad population of galaxies, they produce remnants that are clearly thicker than the Milky Way within ~ 500 pc of the disk plane. Empirically, the Galaxy appears to be deficient in stellar mass and angular momentum when balanced against a sample of local spiral galaxies (Hammer et al. 2007), further motivating the need for a focused program that constrains the Milky Way’s dark disk specifically, rather than relying on general cosmological expectations.

We extend the methodology of PKB09 and use high-resolution simulations to study dark disk production. Our main observational constraint comes from observed kinematic and spatial properties of the old (~ 10 Gyr) thick disk of the Milky Way, which comprises at most $\sim 20\%$ of the total mass of the Galaxy (*e.g.* Jurić et al. 2008). We initialize stellar disks that are consistent with the observed properties of the Milky Way today and consider the impact of fairly massive, cosmologically common accretion events. This approach is conservative: by initializing a disk that is as massive as the Milky Way disk today, we are exploring a case that is both more

resistant to heating and more efficient in capturing dark matter from the accreted satellite than any realistic progenitor of the Milky Way’s thick disk. More generally, by focusing on the oldest, thickest, and hottest stellar component of the Galactic disk, we are able to provide a most conservative constraint on the Milky Way’s merger history.

The heating of the initial disk and the creation of the dark disk are intimately connected, since heating requires the transfer of kinetic energy from the incoming satellite to the disk. For a fixed set of orbital parameters, more massive accretion events produce more stellar heating, and they also deposit more dark matter into a disk-like configuration. The transfer of kinetic energy depends on how close the satellite gets to the disk and its orbit about the disk; a closer and slower orbit results in larger heating and concomitantly larger stripping of dark matter from the satellite by the tides of the Milky Way. Thus, by comparing the heated stellar disk to the observed Milky Way thick stellar disk, we are able to bound the amount of coherently rotating dark matter that is deposited during the disruption of a large satellite galaxy.

As alluded to above, the Milky Way has both a thin and thick disk (Gilmore & Reid 1983), with the latter component being significantly hotter and thicker than the former. By comparing the stellar remnants in our simulations with those of the Galactic thick disk implicitly, we allow for the possibility that the thin disk of the Milky Way is regrown later through fresh accretion. While the regrowth of a thin disk could potentially act to make the heated disk thinner, it cannot make the heated disk colder. Thus our constraints based on the resultant velocity ellipsoid are the most robust.

The majority of the accretion events we consider have mass ratios $M_{\text{sat}}:M_{\text{host}} = 1:10$. This type of merger represents the dominant mode by which dark matter halos grow in Λ CDM models (Purcell et al. 2007; Stewart et al. 2008). They are also the most relevant for the formation of co-rotating dark disks, because more massive mergers are both quite rare and catastrophically destructive to primary disks, while smaller mergers are less heavily affected by dynamical friction and leave behind much less dark matter (we explore such a case below). Thus the 1:10 events we consider here are both cosmologically common and capable of producing a co-rotating dark disk without completely destroying the primary galaxy. Note that while a number of less massive mergers may incrementally build up a thick disk (see Read et al. 2008), they will not produce a coherently rotating dark disk unless the angular momenta contributed by the individual accretion events also coincide constructively. This tendency toward a series of prograde accretions is not found in Λ CDM halos, at least for the few merger histories that have been explored in detail (Kazantzidis et al. 2008).

In addition to collisionless experiments, we perform a hydrodynamical simulation in which the primary galaxy also hosts a gaseous disk, (a much more thorough treatment of these and similar results can be found in Kazantzidis, Purcell, & Bullock 2009, in preparation; see also Moster et al. 2009) to determine whether this component plays a substantial role in the formation of a dark disk. We find that our results do not depend sensitively on the presence of gas as we have modeled it, though we

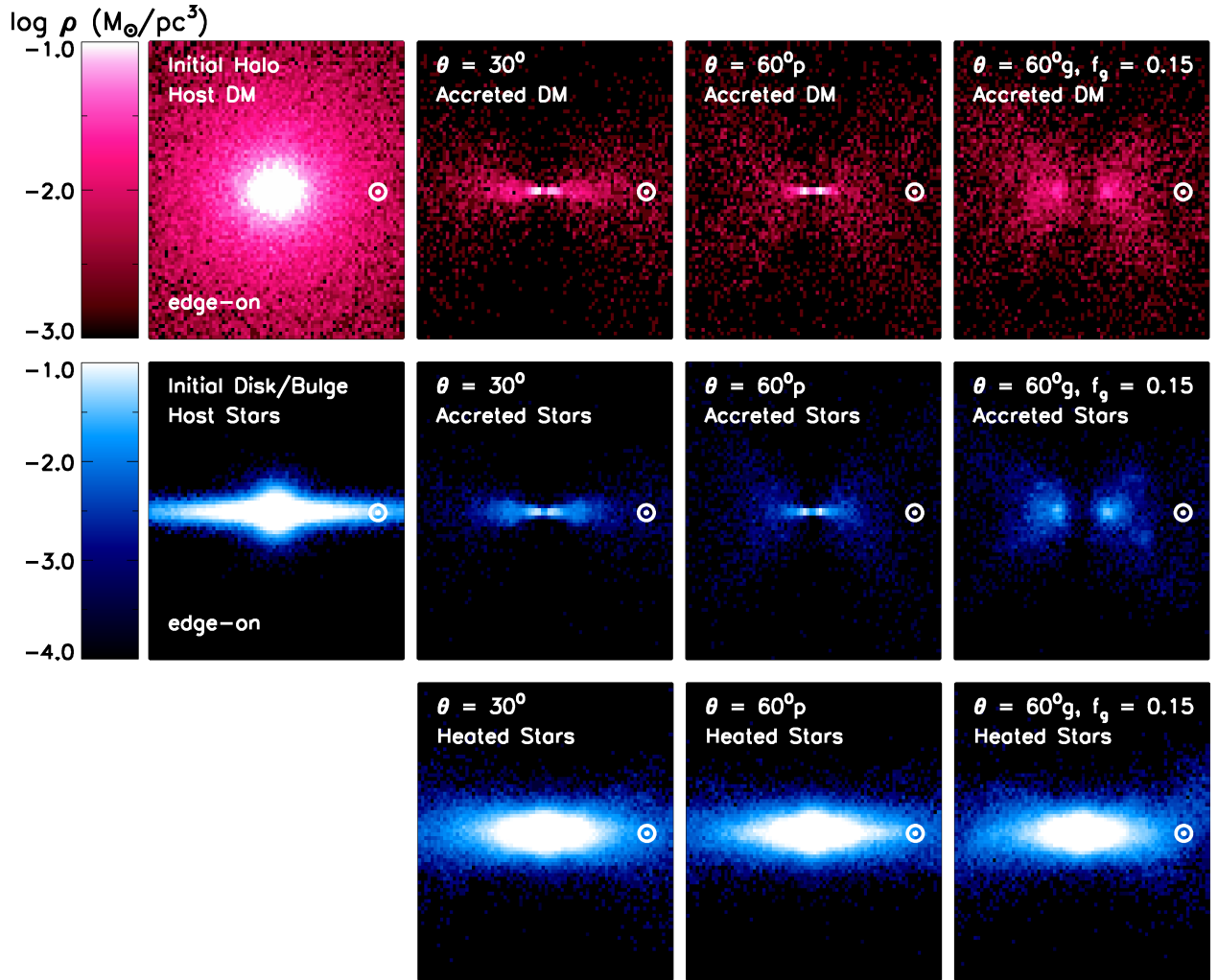


FIG. 2.— The three-dimensional dark matter density (*top panels*) and stellar density (*middle panels*) contributed by the accreted satellite galaxy for a selection of orbital conditions, viewed edge-on with respect to the primary galactic stellar disk and calculated in a vertical slice with a thickness of 1 kpc which passes through the center of the galaxy. For reference, the host galaxy’s structure is mapped in the *left panel* of each figure group and the density maps of the heated primary disk stars are shown in the *lower panels*; each box is 20 kpc on a side and the solar position is marked with \odot .

caution that the treatment of ISM gas physics in galaxy simulations remains uncertain. Based on our implementation, the presence of gas does not curtail the heating of a primary disk that occurs during dark disk creation.

2. METHODS

In a suite of high-resolution collisionless simulations, PKB09 investigated the response of a galactic disk to the infall of cosmologically-common accretion events involving satellites with one-tenth the mass of the host halo. For our primary system, we focus here on the Galaxy 1 model from PKB09, which is a good match to the Milky Way today, and should provide a higher probability of dark disk creation via satellite dragging than any presumably less-massive progenitor of the Galaxy at higher redshift. We now provide a brief overview of our simulations and refer the reader to PKB09 for a more complete discussion of the methods and results regarding the morphological and dynamical changes undergone by stellar disks in response to these accretion events.

Our primary galaxy is constructed according to the fully self-consistent distribution functions prescribed by Widrow et al. (2008) and is therefore an equilibrium so-

lution to the coupled collisionless Boltzmann and Poisson equations. The model’s stellar disk is initialized with an exponential scale length $R_d = 2.84$ kpc and a vertical distribution described by a sech^2 function with scale height $z_d = 0.43$ kpc, containing 10^6 particles with a total disk mass $M_{\text{disk}} = 3.6 \times 10^{10} M_\odot$. The massive central bulge follows a Sérsic profile of effective radius $R_e = 0.58$ kpc and index $n = 1.118$, and has a mass $M_{\text{bulge}} = 9.5 \times 10^9 M_\odot$ distributed among 5×10^5 particles. These stellar components are embedded in a dark host halo composed of 4×10^6 particles which follow the canonical NFW density profile of Navarro et al. (1996), with scale radius $r_s = 14.4$ kpc and virial mass $M_{\text{host}} \simeq 10^{12} M_\odot$. This particular set of parameters was chosen in order to minimize secular effects such as bar formation, as well as artificial heating induced by the interaction of disk particles with more massive halo particles.

The abscissa of Figure 1 as well as the top row of Table 1 denote the infall models we consider. Every simulation tracks the infall of a satellite galaxy modeled within a subhalo of virial mass $M_{\text{sat}} \simeq 10^{11} M_\odot$ at

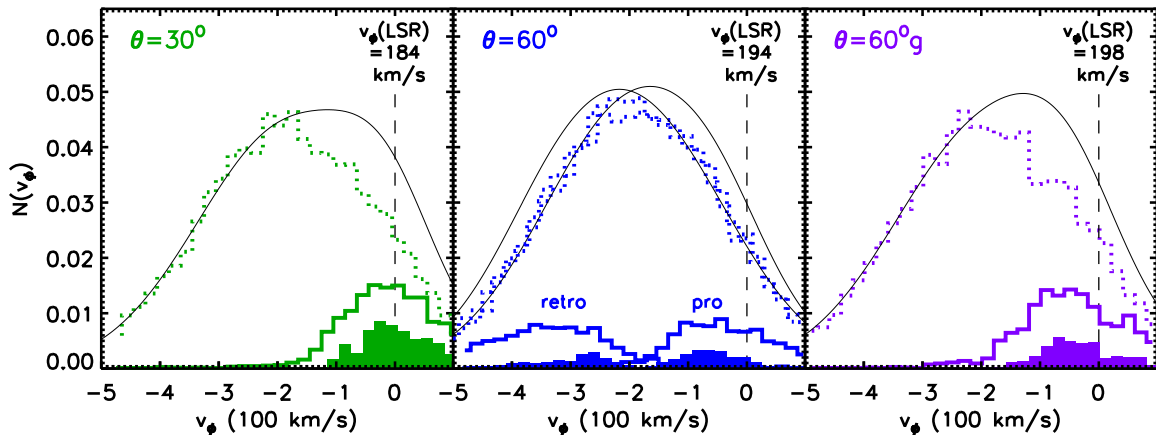


FIG. 3.— Rotational velocity histograms at the solar radius for accreted dark matter (*thick solid*), accreted stars (*shaded region*), and host halo dark matter (*thin dotted*) for infall inclinations corresponding to those shown in Figure 2, calculated with respect to the local standard of rest defined by the rotation speed v_{LSR} of the primary galactic stellar disk. The dark matter values are normalized in each bin to the total number of dark particles in the area defining the solar neighborhood; the number of accreted stars in each bin is normalized to the total number of stars in the same region. In each panel, the *thin solid* line represents the sum of the two Gaussians representing dark matter in the host halo and from the accreted subhalo.

$z = 0.5$. The satellites are each composed of 9×10^5 particles in a density structure well fitted by an NFW profile with concentration $c_{vir} \simeq 14$, and contain a stellar mass $M_* = 2.2 \times 10^9 M_\odot$ distributed among 10^5 particles in a spheroid with Sérsic index $n \sim 0.5$. The stellar masses for the satellite galaxies are drawn from the model of Conroy & Wechsler (2009), which describes the redshift-dependent connection between the observed spatial abundance of galaxies and the corresponding abundance of predicted dark matter halos. Fiducially, we investigate five orbital infall inclinations, including four prograde orbits with $\theta = (0^\circ, 30^\circ, 60^\circ_p, \text{ and } 90^\circ)$ and one retrograde 60°_r orbit. The satellites are initialized 120 kpc from the host halo center, and we set our initial orbital vectors according to the distribution of substructure accretions drawn from cosmological simulations (Benson 2005; Khochfar & Burkert 2006), with radial and tangential velocity components equal to $v_r = 116 \text{ km s}^{-1}$ and $v_t = 77 \text{ km s}^{-1}$ respectively. Additionally, in a model we designate 0°_s , we investigate a case where the same satellite galaxy is traveling more slowly than in the fiducial 0° case, with $v_r = 58 \text{ km s}^{-1}$ and $v_t = 38.5 \text{ km s}^{-1}$; these orbital parameters correspond roughly to the lower 1σ limit of Benson (2005).

To test the effect of a full treatment of hydrodynamics on the morphological and dynamical changes induced by an accretion event, we repeat the simulation involving a massive satellite galaxy infalling along a prograde orbit with an inclination of 60° (hence the designation 60°_g), having converted a modest fraction $f_g = 15\%$ of the initial primary galaxy’s star particles into a gaseous component with the same density structure as the stellar disk. Our hydrodynamical prescription includes atomic cooling for a primordial mixture of hydrogen and helium, and the star formation algorithm is based on the work of Katz (1992), in which gas particles in cold and dense regions form star particles at a rate proportional to the local dynamical time; star formation occurs when the gas density exceeds 0.1 cm^{-3} and the gas temperature drops below $1.5 \times 10^4 \text{ K}$. Supernova feedback is implemented according to the blast-wave model described in Stinson et al. (2006), in which the energy deposited by a Type-II su-

pernova into the surrounding gas is 4×10^{50} ergs. This parameter set produces realistic galaxies in cosmological simulations (Governato et al. 2007). Again we refer the reader to Kazantzidis, Purcell & Bullock (2009, in preparation) for more details regarding the suite of experiments to which this current test case belongs.

As a test of the fractional contribution made by a much smaller satellite galaxy, we simulate an additional accretion event with identical orbital parameters to the fiducial infall, involving a subhalo of mass $M_{sat} \sim 4 \times 10^{10} M_\odot$, i.e. with mass ratio 1:25. For this case, we choose a planar subhalo orbit ($\theta = 0^\circ$) in order to maximize the likelihood of dark disk formation. However, this experiment resulted in a trivial increase ($\lesssim 1\%$) in the fraction of dark matter in the solar neighborhood, and is thus not listed in Table 1.

3. RESULTS

3.1. Gross Comparisons to the Galactic Stellar Disk

We summarize in Figure 1 the observable properties of our initial and remnant stellar disks, with each model indicated by name along the horizontal axis. The upper panel shows the disk scale height z_d , derived from fitting the minor axis surface density profile at a defined solar radius ($R_\odot = 8 \text{ kpc}$), using the two-component form

$$\Sigma(z) = \Sigma_d \text{sech}^2(z/z_d) + \Sigma_{diffuse} \text{sech}^2(z/z_{diffuse}). \quad (1)$$

This decomposition provides a minimum estimate of the resultant disk scale height (z_d) by allowing for a secondary, much thicker component ($z_{diffuse}$), which dominates at large height and low surface brightness. Generally, we find significant variance in these values with orbital inclination angle; the disk scale height $z_d \sim 1 - 2 \text{ kpc}$, while the faint component typically has $z_{diffuse} \sim 4 - 7 \text{ kpc}$. Note that the initial thin disk of the primary galaxy has been destroyed: our minimal scale heights are comparable to or larger than the Galactic thick disk scale height, as demonstrated in the comparison of Figure 1, where observed scale heights for the Milky Way thin and thick disks are shown as shaded horizontal bands. These values are drawn from Jurić et al. (2008), in which an exponential disk scale height is pre-

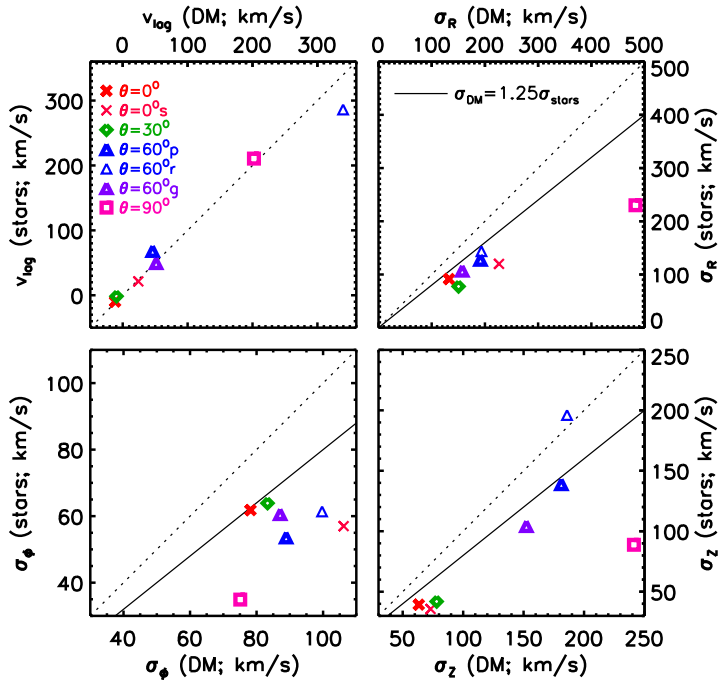


FIG. 4.— Correlations between the kinematic properties of dark matter and stars accreted onto the primary galaxy during satellite infall. The *upper left* panel shows the amount v_{lag} by which each species of accreted material lags the rotational speed of the primary galactic disk; negative (positive) quantities indicate faster (slower) rotation than the local standard of rest as defined by the mean stellar velocity of disk stars in the solar neighborhood. The remaining three panels plot each axis of the velocity ellipsoid for both species. In all figures, the ordinate marks the values for accreted stars, while the abscissa denotes the corresponding values for accreted dark matter; the *dotted* line defines where the two values are equal, while the *solid* line forms the upper bound $\sigma^{DM} = 1.25\sigma^{\text{stars}}$ of an envelope which roughly contains the simulation results.

sented; we convert this value here to a sech^2 scale height such that the two vertical surface density profiles decrease by roughly the same amount within ~ 1 scale height of the disk plane². The total three-dimensional velocity dispersion $\sigma_{\text{tot}} = (\sigma_R^2 + \sigma_\theta^2 + \sigma_\phi^2)^{1/2}$ of each disk at the solar neighborhood is presented in the bottom panel of Figure 1. The significant increase in this quantity from the initial model to the resultant disk betrays the extraordinary heating undergone by the primary disk during the merger. The shaded bands again reflect observed velocity dispersions for the Milky Way thin and thick disks, as drawn from Nordström et al. (2004) and Soubiran et al. (2003), respectively.

If we associate our remnant disks with the Milky Way thick disk, most of our resultant systems are thicker and hotter than the Galaxy. This comparison is particularly constraining for two reasons. First, the age distribution of stars in the *thin disk* includes stars that are 8-10 Gyr old, suggesting that any merger of this kind must have happened well before $z \sim 1$ (when the primary disk was even smaller and less able to cause significant dragging into the disk plane). Moreover, while regrowth of a new

² Note that much of the relevant literature, including *e.g.* Moster et al. (2009), uses the typical conversion factor of two, which is only valid at heights much larger than the scale height of the disk. Our conversion method captures more accurately the behavior of the surface brightness profile at heights comparable to and smaller than the disk scale height.

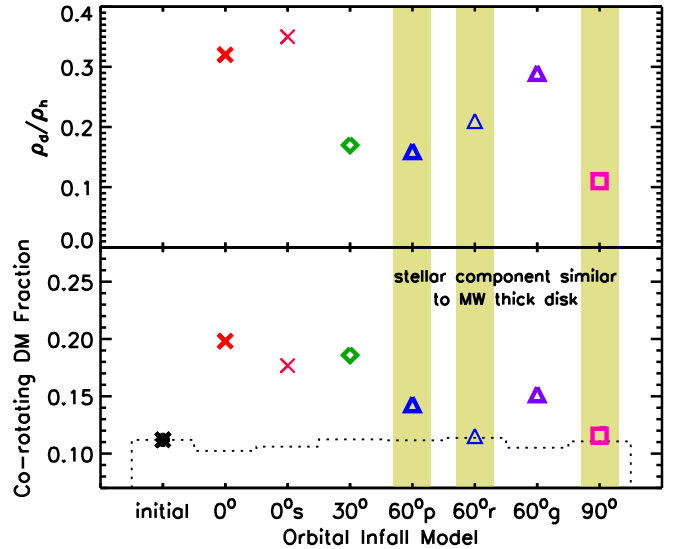


FIG. 5.— Similar to Figure 1, morphological and dynamical properties of the final accreted dark disks at the solar neighborhood for each fiducial orbital infall condition: the local density ratio ρ_d/ρ_h (*upper panel*), and the fraction of local dark matter moving slowly ($|v_{\text{lag}}| \leq 50$ km/s) with respect to the stellar disk’s rotational speed (*lower panel*). In the latter case, the *thin dotted* histogram denotes the contribution to the fraction of slow-moving dark matter made by the initial host halo, while the colored points indicate the sum of this component and the amount of co-rotating dark matter deposited by the accreted satellite galaxy. The shaded regions correspond to the orbital infall models that produce stellar remnants with morphology and kinematics similar to the Galactic thick disk, as demonstrated by Figure 1.

disk could potentially reduce the scale height of the thickened disk, it would not reduce the velocity dispersion of the stars. Only the prograde and retrograde 60° orbits and the 90° degree orbits result in a system that is marginally viable, both morphologically and dynamically.

3.2. Morphological and Kinematic Characterizations of the Dark Disk

Each of the merger simulations provides an accreted dark component and an accreted stellar component, but the nature of these components depends sensitively on the interaction, as illustrated in Figure 2 for three of our simulations. For reference, the upper left panel presents a central slice of the dark matter density in the primary galaxy’s host halo prior to the accretion, the middle left panel shows a slice in the stellar distribution in the primary galaxy, and the lower panels represent the heated stars belonging to the original disk only. The three columns on the right for the upper two rows display the resultant distributions of accreted dark matter and accreted stars; as might be expected, the lower-latitude event produces the most disk-like accreted dark matter morphology, with a qualitatively similar accreted stellar distribution that is somewhat more rotationally supported owing to the fact that the stars are more tightly bound in the satellites than the dark matter. As noted in Table 1, the low-latitude simulations also produce the largest fractional density ρ_d/ρ_h of accreted dark matter compared to background halo dark matter in the solar neighborhood³. High-latitude events create less

³ Throughout this work, we define the solar neighborhood as the area between galactocentric radii $7 < R < 8$ kpc and bounded

discernible dark disks at the solar position and deposit proportionally less dark matter there; we also note that our test model involving the planar infall of a satellite galaxy with mass ratio $M_{\text{sat}}:M_{\text{host}} = 1:25$ evolves over a much longer timescale than that of the fiducial models, and also results in a negligible contribution to the local dark matter quotient, indicating that even a multitude of small subhalos with similar orbits may not be able to form a significant dark disk. For the models with mass ratio $M_{\text{sat}}:M_{\text{host}} = 1:10$, Table 1 provides dark disk and accreted stellar disk scale heights at the solar neighborhood, as computed by fitting a sech^2 profile.

An additional characterization of interest is the velocity distribution of the dark disk component. It is useful to parametrize the dark matter in the solar neighborhood of our simulations with a double Gaussian distribution that represents the original host and accreted subhalo material:

$$f(v_R, v_\phi, v_z) = f_{\text{host}}(v_R, v_\phi, v_z) + f_{\text{acc}}(v_R, v_\phi, v_z), \quad (2)$$

where in each term

$$f(v_R, v_\phi, v_z) = A e^{-\sum (v_i - \bar{v}_i)^2 / 2\sigma_i^2}. \quad (3)$$

The sum involves each velocity component, $i = R, \phi, z$. We work in a frame that co-rotates with the resultant stellar disk such that the host halo produces a net dark matter wind in the ϕ direction that is close to the primary galaxy rotation speed $(\bar{v}_\phi)_{\text{host}} \sim -200$ km/s and $\bar{v}_R = \bar{v}_z \sim 0$. Accreted matter can co-rotate or anti-rotate with the stellar disk and we quantify this rotation in accreted material by the lag speed $v_{\text{lag}} = -\bar{v}_\phi$, such that a zero lag corresponds to precise co-rotation, while a positive lag trails the stellar disk and a negative lag means that the dark disk is rotating faster than the stellar disk. The resultant velocity distribution parameters for each accreted component in our simulations are presented in Table 1.

In Figure 3, we show the collapsed distributions in rotational velocity v_ϕ for the background host halo as well as accreted dark matter, along with our double-Gaussian fit to the total amount of dark matter in the solar neighborhood, for the same three resultant galaxies that were illustrated in Figure 2: 30°, 60°p, and 60°g. The center panel also presents the velocity distribution for the 60°r retrograde merger. The filled histograms in each panel show the velocity distributions for accreted stars, normalized relative to the total stellar mass at the solar location. Two points are immediately apparent; first, that lower-latitude accretion events produce smaller lag velocities in both accreted species, and secondly that the lag speed of accreted stars grossly mimics that of the accreted dark matter for accretion events at all latitudes.

3.3. Correlating the Dark and Stellar Disks

The kinematic relationship between the accreted dark and stellar disks (a phenomenon also reported by Read et al. 2008, 2009) is important because it may provide an avenue to constrain the dark disk velocity distribution via observational studies that can isolate an accreted stellar component. In Figure 4, we show the

vertically by $|z| \leq 2$ kpc; we also note that variance in these boundaries does not lead to significantly altered results.

correlations between accreted dark matter and accreted stars in each velocity dispersion component, as well as the rotational lag speed, which correlates very well between the two accreted species. We also note that the velocity dispersion of accreted stars generally provides a lower limit on the velocity dispersion of the dark disk in each directional component; the correlations in Figure 4 indicate that dark matter dispersions are consistently at least a factor of 1.25 larger than their stellar counterparts.

Though not explicitly shown here, we also find a connection between the velocity-ellipsoid axis ratio σ_z/σ_R of the accreted dark matter and that of the stars formerly belonging to the satellite galaxy, in that the two collisionless events involving the high inclination angle of $\theta = 60^\circ$ both have vertical to radial velocity dispersion ratios of approximately unity for all accreted material, while the velocity ellipsoids resulting from the low-latitude events are significantly more oblate, with both stellar and dark axis ratios roughly equal to ~ 0.5 : a similar value to that obtained observationally for the Galactic solar neighborhood (Gomez et al. 1990; Nordström et al. 2004). It should be noted here that the polar infall results in a final velocity-ellipsoid axis ratio coincident with that of the low-latitude events, due to a very large dispersion in the radial velocity of both accreted species in this case.

3.4. Summary of Results

We use two simple metrics to characterize our main results in Figure 5; as in Figure 1, each model is indicated along the horizontal axis. The upper panel presents the accreted dark matter fraction ρ_d/ρ_h in the solar neighborhood; the lower panel presents the fraction of local dark matter that is roughly co-rotating with the stellar disk, which is potentially the most salient characteristic of an accreted dark disk. Specifically, we define the latter quantity to be the fraction of accreted dark particles with rotational speeds within 50 km/s of the stellar disk’s velocity, *i.e.* $|v_\phi - v_{LSR}| \leq 50$ km/s. Note that by this definition, even the initial spherical halo has a non-zero co-rotating dark matter fraction; for reference, the dotted line in the lower panel of Figure 5 shows the fraction of dark matter particles initially from the background halo that are co-rotating with the stellar disk in the final simulation snapshot.

As might be expected, the most significant dark disks form during the planar accretion events 0° and 0°s, which respectively produce 32% and 35% accreted dark matter fractions in the solar vicinity and factors of 1.7 and 1.4 enhancements in the co-rotating dark matter fraction. However, these planar events also produce stellar disks that are much hotter than the thick disk of the Milky Way (as shown in Figure 1), indicating that these cases are not appropriate baseline models for the Galaxy. Though not evident in Figure 1, the slower orbit actually produces more radial heating than the fast orbit (see Table 1) and is therefore more discrepant with the Milky Way thick disk velocity structure than the standard orbit.

The three shaded bands in Figure 5 highlight the three model cases that produce stellar disks marginally consistent with the thick disk of the Milky Way, when considering morphology as well as dynamical temperature. The most optimistically viable model for a dark disk is

the 60-degree prograde orbit, which results in a 16% accreted dark matter contribution and a 14% co-rotating dark matter fraction; the latter quantity represents a $\sim 30\%$ increase compared to the co-rotating dark matter fraction in the smooth halo case. As noted in Table 1, the dark disk scale height in this case is $z_d = 4.6$ kpc and lags the LSR with $v_{\text{lag}} = 46$ km/s.

Although the thick disk we produce is obviously more massive than the Galactic thick disk, the similarity in morphology and kinematics motivate us to move beyond limits, and speculate on the properties of the actual dark disk in the Milky Way. Given the range of parameters probed here and in Read et al. (2008), and operating under the assumption that the Milky Way’s thick disk was formed in an event similar to the type we simulate here, we expect that the real Galactic dark disk contributes roughly 10% to the local dark matter density. As we discuss below in §5, such a dark disk does not significantly enhance the possibility of direct detection of dark matter; however, it will be important to include in any detailed analysis aimed at interpreting an observed WIMP detection signal. Moreover, such a dark disk may provide a detectable morphological signature towards the Galactic center in experiments designed to indirectly detect dark matter via its self-annihilation products.

4. COMPARISON TO PREVIOUS WORK

In a recent effort to quantify disk heating in a Λ CDM context, Read et al. (2008) used simulations similar to those presented here in order to show that massive satellite accretion events involving a Galactic-type thin disk not only produce thick stellar systems but also result in the deposition of accreted dark matter into a disk-like component that co-rotates to some degree with the primary galaxy. Specifically, they analyzed dark disk formation during the infall of various subhalo types (of particular interest here are their LMC and LLMC models, representing satellite galaxies with total mass $M_{\text{sat}} \simeq 2.4 \times 10^{10}$ and 1.0×10^{11} respectively), finding that for low-inclination mergers, the resulting density ratio of accreted dark matter to that of the background host halo in the solar neighborhood was $\rho_d/\rho_h = 0.22$ for the smaller subhalo and 0.42 for the more massive satellite that corresponds closely to our fiducial infalling system. In the follow-up analysis of cosmological simulations of Milky-Way-type disk galaxies (Read et al. 2009), the authors found similar results for systems with a wide range in accretion history activity, showing that several massive mergers at late times can result in a dark disk with local density similar to that of the host halo itself.

Although our simulated phenomena are qualitatively similar to those presented by Read et al. (2008), there are two key points of distinction to be drawn. The two methods are only significantly discrepant in the choice of initial radii and velocities of the infalling satellites. Our work adopts satellite galaxy velocity vectors drawn from subhalo infall distributions found in cosmological simulations, and thus we set the initial position of the subhalo far (~ 120 kpc) from the host halo’s center in order to minimize the sudden change in potential felt by the primary galactic disk and also to imitate the cosmological velocity conditions, which are measured at the host’s virial radius. In contrast, the infalling satellites of Read et al. (2008) begin much closer (~ 30 kpc) to the

primary disk’s center and involve subhalos traveling at speeds slower than our fiducial initial velocity by roughly fifty percent; slightly faster than our 0° ’s case. The authors motivate the choice of a slow orbit at a small initial Galactocentric apocenter by suggesting it replicates the orbital parameters of satellites found in a loose group environment that is accreted onto a Galaxy-sized host. However, it still remains to be shown that such a velocity vector at ~ 30 kpc can arise naturally for a massive satellite within a cosmological setting. Moreover, any process that would act to bring a subhalo to such a low energy state in the disk plane would almost certainly heat the primary disk to a degree unallowable by observations.

The difference in initial conditions may be largely responsible for the small systematic differences between our simulated dark disk results and those of Read et al. (2008). While our maximal local density ratio is $\rho_d/\rho_h \sim 0.35$, they find 0.42 in their experiment labeled LLMC- 10° , an accretion event involving a subhalo of similar mass. The methodological variance may also explain why our disks are slightly dynamically hotter. Our 0° case has $\sigma_{\text{tot}} \sim 117$ km/s and our 0° ’s case has $\sigma_{\text{tot}} \sim 110$ km/s, while their LLMC- 10° model has $\sigma_{\text{tot}} \sim 105$ km/s. It is important to emphasize, however, that both sets of simulations find resultant thick disks that are hotter than the observed thick disk of the Milky Way, which has a total dispersion of just ~ 85 km/s. Therefore, in a broad sense, we agree that these disks are not ideal analogues to the Milky Way.

We note that a more substantial dark disk component could emerge following multiple similar accretion events, as investigated in cosmological simulations of Galaxy-sized disks by Read et al. (2009), but such a series of late-time mergers cannot be reconciled with the relatively thin disk of the Milky Way. Unfortunately for experiments aimed at detecting local dark matter, the quiescent Galactic accretion history favored by our result indicate that the relevant observable quantities are probably far less affected by a dark disk than we might have hoped.

5. DISCUSSION AND INTERPRETATION

In our experiments, we have adopted assumptions throughout that maximize the likelihood for producing a dark disk remnant and for preserving a thin, cold disk by initializing a primary disk that is as massive as the Milky Way disk today. This approach is quite conservative because we compare the heated stellar remnant to the old *thick disk* of the Milky Way, which is at least five times less massive than our primary system (*e.g.* Jurić et al. 2008, and references therein). We have argued that the dark disk formed in our 60° prograde merger case provides a fair limit on the properties of an underlying accreted dark component of our Galaxy, with a local contribution $\rho_d/\rho_h \simeq 0.15$ that is at the low end of dark disk contributions estimated by Read et al. (2008) for Milky Way type galaxies in Λ CDM.

Based on this limit, we expect that nuclear recoil experiments designed to directly detect local dark matter would only receive small boosts to the event rate, preferentially at lower energies. Dark disk fractions of $\rho_d/\rho_h \sim 10\%$ were explored by Bruch et al. (2009a), who found an order unity enhancement in the differential event rate at keV recoil energies for a 100 GeV dark mat-

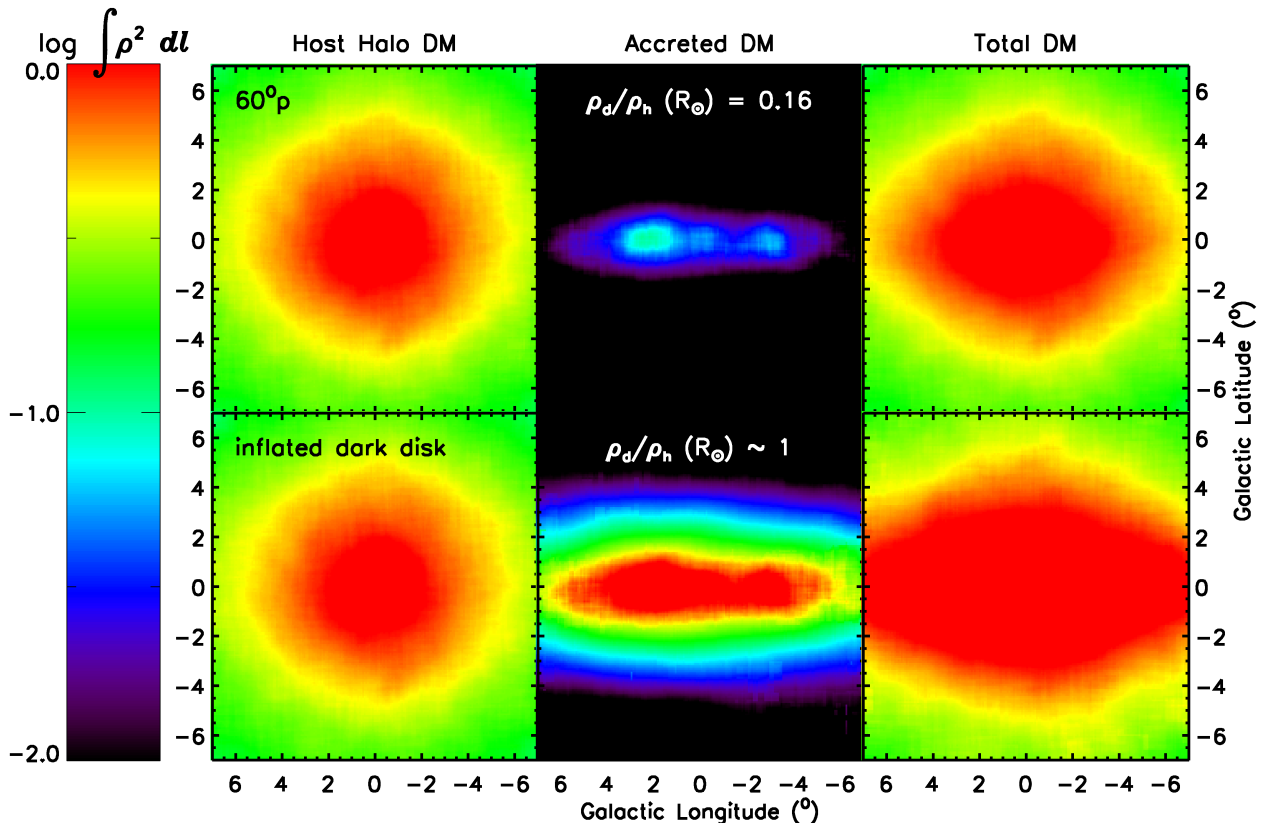


FIG. 6.— The dark matter annihilation signal in Galactic coordinates, mapped with a color logarithmically proportional to the integrated square of the particle density along a line of sight toward the center of the galaxy, following the prograde satellite galaxy infall with inclination $\theta = 60^\circ$. Note that the combined signal (*right panels*) is noticeably more oblate than the host material alone (*left panels*; shown *after* the accretion event); the accreted dark matter (*center panels*) contributes roughly $\sim 10 - 25\%$ of the annihilation rate at Galactic longitudes $\sim 5^\circ - 10^\circ$. In the lower set of figures, we test the effect on the total annihilation signal for a hypothetical dark disk with a local density ratio at the solar neighborhood $\rho_d/\rho_h \sim 1$; this boost is also an $O(1)$ effect, contributing $\sim 50\%$ of the total signal over the same range in longitude. We have argued that such a large dark disk component would likely have to form through secular processes unrelated to satellite accretion events.

ter particle. For a TeV mass dark matter particle, such an enhancement would be present at higher energies (accessible to CDMS-II). While an order unity enhancement will not significantly impact the event rate, Bruch et al. (2009a) showed that the phase of the annual modulation signal is sensitive to both the dark disk and the mass of the dark matter particle. The phase of the annual modulation signal produced by the dark disk depends on the motion of the Sun relative to the dark disk. The phase of the modulation of the total event rate in a given energy window depends on both the mass of dark matter particle and the dark disk fraction. If the dark disk fraction is bracketed from the lower end, this will result in a prediction for the phase given a dark matter particle mass. This may be testable at future detectors if a positive signal is seen. In addition, these results also imply that directional detectors should see the WIMP wind direction change as a function of recoil energy, the details of which would depend on the energy window, the mass of the WIMP, the dark disk fraction and the motion of the Sun with respect to the dark disk.

An increase in the local number density of particles that co-rotate with the Sun will also enhance WIMP capture in the Sun and the Earth. These captured particles self-annihilate into standard model particles, including neutrino pairs. Thus a larger co-rotating fraction of dark matter will result in a larger neutrino flux potentially

observable with experiments like Super-Kamiokande and IceCube. In detail, the capture rate depends sensitively on ρ_d/ρ_h , the dark disk lag speed v_{lag} , and the velocity dispersion of the dark disk. The timescale for capture of WIMPs at Earth is small compared to the age of the planet and hence the WIMP density in the Earth has not yet reached equilibrium. In the Sun, as shown by Bruch et al. (2009b), the situation is the opposite for most regions of parameter space and the number of WIMPs would have reached an equilibrium value. Thus the annihilation rate of WIMPs inside the Earth is proportional to the capture rate squared, while in the Sun it is equal to half the capture rate (given the equilibrium condition there). Bruch et al. (2009b) show that this leads to two to three orders of magnitude enhancement in the flux from the Earth and an order of magnitude enhancement in the flux from the Sun for $\rho_d/\rho_h = 1$ and an assumed isotropic Gaussian velocity distribution for the dark disk with lag $v_{\text{lag}} = 50$ km/s and 1-D dispersion $\sigma_d = v_{\text{lag}}$. They also consider dark disk parameters $\rho_d/\rho_h = 0.25$ and $\sigma_d = 100$ km/s and state that this does not lead to a large boost in the signal, owing primarily to the large velocity dispersion. By comparison, our simulated prograde accretion event with $\theta = 60^\circ$ results in a local density ratio of 0.15, velocity dispersion $\sigma_\phi \simeq 90$ km/s, and similar lag speed $v_{\text{lag}} \simeq 50$ km/s. Thus we do not expect large boosts to the neutrino flux

from the Earth or the Sun, and our results imply that the likelihood of WIMP detection through this indirect channel is not significantly increased due to an accreted dark disk.

Although the prospects for direct detection and indirect detection via WIMP capture are not significantly altered by the accreted dark disk, we note that the accreted dark matter distribution is relatively more prominent toward the center of the galaxy, where most of the satellite galaxy’s material settles. The center of the Galaxy is a prime target for experiments aimed at detecting dark matter indirectly via high energy annihilation products (Bergström et al. 1998), as the flux scales proportionally to the square of the WIMP density. In Figure 6, we view the halo’s center from the vantage point of the solar neighborhood, after the prograde 60° satellite infall, and estimate the annihilation signal at Earth by integrating ρ^2 along lines of sight. We notice immediately that while the host’s dark matter has retained approximate sphericity (left), the combined signal (right) which includes the accreted subhalo material (middle) has a significantly more oblate contour. Approximately $\sim 10 - 25\%$ of the total ρ^2 contribution at galactic longitudes between 5° and 10° comes from accreted dark matter. As in the case of direct detection, the dark disk does not significantly change the likelihood of detection; however, if there is a positive detection, then our results provide motivation to search for a disk-like component with scale height and length that are different from that of the Milky Way thin disk.

Our focus in this work has been on the scenario of Read et al. (2008), who showed that dark disks could be created via satellite accretion events. We have argued that under this scenario, the relative importance of the accreted dark disk can be constrained via detailed comparison to the properties of thick disk stars in the Galaxy and that this constraint limits the dark disk’s density contribution to $\sim 0.2\rho_{\text{halo}}$ in the solar neighborhood. However, it is interesting to consider the theoretical possibility that a dark disk with density ratio $O(1)$ could form in response to some other process that did not heat the disk. For example, one could imagine that large infalling gas clouds could transfer angular momentum to the dark matter, creating a disk-like dark component without disturbing the primary disk significantly. Such a process may not be easy to arrange, given the large amount of angular momentum transfer required to produce a co-rotating dark disk as well as the fact that observed disk galaxies seem to require something close to angular momentum conservation.

Nonetheless, it is an instructive exercise to determine the effect of an $O(1)$ dark disk on indirect detection signals. To investigate this, we have scaled the local density ratio for the 60° prograde case such that $\rho_d/\rho_h = 1$, and the resultant annihilation signal’s sky map is shown in the lower panels of Figure 6. The disk-like nature of the signal is clearly apparent and could be easily distinguished if any dark matter self-annihilation is observed toward the center of the Galaxy. Therefore, if such a dark disk could somehow form without involving satellite accretion events, it would be discernible through indirect detection experiments. Coupled with the boost in the direct detection signal that is expected for such an $O(1)$ dark disk (Bruch et al. 2009b), the jointly observ-

able consequences of such a component would be significant.

In a similar vein, it is worth noting that the quantity of interest for direct detection experiments is the fraction of slow-moving dark matter particles. From Figure 5, we see that the 30° case shows an order unity enhancement in slow-moving dark matter particles, and Figure 1 shows that this run produces a disk that is only marginally hotter than the thick disk of the Milky Way. However, the scale height of the disk is considerably larger. One may, however, hypothesize that a later stage of disk formation could change the disk scale height substantially without heating the stars further. Therefore, we urge the reader to keep in mind that $O(1)$ enhancement in slow-moving particles is possible in the accreted dark disk scenario of Read et al. (2008), but that the expected velocity dispersion in the ϕ direction is still large – in our 30° case, it is 83 km/s (see Table 1).

In this work we have argued that within the context of the accreted dark disk scenario of Read et al. (2008), it is likely that the dark disk of the Milky Way contributes approximately 10 – 20% to the local dark matter density. If so, then its presence may be important to include in any attempt to interpret a detection signal of WIMP dark matter in the solar neighborhood and for the indirect detection signal from the Galactic center. Given this, it will be important to constrain the dark disk to a higher degree of accuracy. Both Read et al. (2008) and we have demonstrated that there is a significant dynamical relationship between dark matter accreted during the infall of a massive subhalo and the stellar mass contributed by that satellite galaxy to the primary system (Table 1 and Figure 4). Therefore one can anticipate constraining the properties of any Milky Way dark disk by isolating a dominant subpopulation of accreted Galactic disk stars, perhaps by some combination of chemical and dynamical tags. For example, if we were to consider the unlikely scenario where the entire thick disk of the Milky Way was deposited by a single accretion event (*i.e.* it is devoid of any pre-existing disk stars), then we may consider the dynamical properties of the Galaxy’s thick disk as a means to constrain the dark disk: $(\sigma_R, \sigma_\phi, \sigma_z) = (63 \pm 6, 39 \pm 4, 39 \pm 4)$ km/s, $v_{\text{lag}} = 51.5$ km/s (Soubiran et al. 2003), and $z_d = 0.90 \pm 0.18$ kpc (Jurić et al. 2008). Under this interpretation, our simulation results would imply that the lag speed of the MW dark disk is ~ 50 km/s and that it must be quite hot, with $1.25(\sigma_R, \sigma_\phi, \sigma_z) \sim (88, 51, 62)$ km/s, and with a very thick $z_d \gtrsim 2$ kpc. These numbers are almost certainly lower limits; as we have shown in Table 1, accreted stellar distributions tend to be both hotter and thicker than the primary disks they heat. If there is any pre-existing disk population associated with the thick disk of the Milky Way, the accreted portion is almost certainly hotter than the composite thick disk values used in our analysis.

Although theoretical predictions based on galaxy formation models as they relate to dark matter detection are still in the nascent stage, it is clear that the standard halo model is insufficiently equipped to allow precise predictions for measurable quantities of interest; scattering rates and flux scalings depend crucially on the presence of locally coherent substructural flows. Observations have thus far been unable to accurately estimate the degree to which the Galactic thick disk’s population

is composed of stars stripped from a satellite galaxy during tidal disruption, as opposed to material heated to ejection from the thin stellar disk (as investigated by Purcell et al. 2009b). In principle, however, a combination of high-precision kinematic measurements and detailed chemical composition data should be able to define a phase-space in which accreted and original stars occupy disparate regions. Placing such dynamical constraints on the population of stars obtained by the Milky Way during a significant accretion event may enable us to identify the kinematics of the dark matter deposited during that same event, thereby placing more stringent limits on the availability of a dark Galactic disk for the purpose of detection experiments.

We thank Justin Read, Laura Baudis, Tobias Bruch, and George Lake for discussions that improved the accu-

racy and clarity of our presentation. Stelios Kazantzidis assisted in the construction of the initial conditions used in this work, and we thank him for allowing us to present the results of our collaborative disk-satellite experiments here, including the hydrodynamical experiment described above. We also thank Larry Widrow and John Dubinski for kindly making available the software used to set up the initial galaxy models. CWP and JSB are supported by National Science Foundation (NSF) grants AST-0607377 and AST-0507816, and the Center for Cosmology at UC Irvine. MK is supported by NSF grant AST-0607746 and NASA grant NNX09AD09G. The numerical simulations were completed primarily on the IA-64 cluster at the San Diego Supercomputing Center, with ancillary experiments performed on the Green-Planet cluster at UC Irvine.

REFERENCES

- Benson, A. J. 2005, *MNRAS*, 358, 551
 Bergström, L., Ullio, P., & Buckley, J. H. 1998, *Astroparticle Physics*, 9, 137
 Bruch, T., Read, J., Baudis, L., & Lake, G. 2009a, *ApJ*, 696, 920
 Bruch, T., Peter, A. H. G., Read, J., Baudis, L., & Lake, G. 2009b, *Physics Letters B*, 674, 250
 Conroy, C., & Wechsler, R. H. 2009, *ApJ*, 696, 620
 Gilmore, G., & Reid, N. 1983, *MNRAS*, 202, 1025
 Gomez, A. E., Delhaye, J., Grenier, S., Jaschek, C., Arenou, F., & Jaschek, M. 1990, *A&A*, 236, 95
 Governato, F., Willman, B., Mayer, L., Brooks, A., Stinson, G., Valenzuela, O., Wadsley, J., & Quinn, T. 2007, *MNRAS*, 374, 1479
 Hammer, F., Puech, M., Chemin, L., Flores, H., & Lehnert, M. D. 2007, *ApJ*, 662, 322
 Helmi, A., White, S. D. M., & Springel, V. 2003, *MNRAS*, 339, 834
 Johnston, K. V., Sackett, P. D., & Bullock, J. S. 2001, *ApJ*, 557, 137
 Jungman, G., Kamionkowski, M., & Griest, K. 1996, *Phys. Rep.*, 267, 195
 Jurić, M. et al. 2008, *ApJ*, 673, 864
 Kamionkowski, M., & Koushiappas, S. M. 2008, *Phys. Rev. D*, 77, 103509
 Katz, N. 1992, *ApJ*, 391, 502
 Kazantzidis, S., Bullock, J. S., Zentner, A. R., Kravtsov, A. V., & Moustakas, L. A. 2008, *ApJ*, 688, 254
 Kochfar, S. & Burkert, A. 2006, *A&A*, 445, 403
 Moster, B. P., Maccio', A. V., Somerville, R. S., Johansson, P. H., & Naab, T. 2009, arXiv:0906.0764
 Navarro, J. F., Frenk, C. S., & White, S. D. M. 1996, *ApJ*, 462, 563
 Nordström, B. et al. 2004, *A&A*, 418, 989
 Peter, A. H. G. 2009, *Phys. Rev. D*, 79, 103531
 Purcell, C. W., Bullock, J. S., & Zentner, A. R. 2007, *ApJ*, 666, 20
 Purcell, C. W., Kazantzidis, S., & Bullock, J. S. 2009, *ApJ*, 694, L98
 Purcell, C. W., Bullock, J. S., & Kazantzidis, S. 2009, *MNRAS*, in preparation
 Read, J. I., Lake, G., Agertz, O., & Debattista, V. P. 2008, *MNRAS*, 389, 1041
 Read, J. I., Mayer, L., Brooks, A. M., Governato, F., & Lake, G. 2009, arXiv:0902.0009
 Smith, P. F., & Lewin, J. D. 1990, *Phys. Rep.*, 187, 203
 Soubiran, C., Bienaymé, O., & Siebert, A. 2003, *A&A*, 398, 141
 Stewart, K. R., Bullock, J. S., Wechsler, R. H., Maller, A. H., & Zentner, A. R. 2008, *ApJ*, 683, 597
 Stinson, G., Seth, A., Katz, N., Wadsley, J., Governato, F., & Quinn, T. 2006, *MNRAS*, 373, 1074
 Widrow, L. M., Pym, B., & Dubinski, J. 2008, *ApJ*, 679, 1239
 Wyse, R. F. G. 2009, *IAU Symposium*, 254, 179
 Villalobos, Á., & Helmi, A. 2008, *MNRAS*, 391, 1806
 Vogelsberger, M., et al. 2009, *MNRAS*, 395, 797

TABLE 1
 PROPERTIES OF ACCRETED DARK MATTER AND STARS IN THE SOLAR NEIGHBORHOOD

Quantity (DM)	Orbital Inclination							Units
	$\theta = 0^\circ$	$\theta = 0^\circ$ -slow	$\theta = 30^\circ$	$\theta = 60^\circ$	$\theta = 60^\circ$ -gas	$\theta = 60^\circ$ -retro	$\theta = 90^\circ$	
ρ_d/ρ_h	0.32	0.35	0.17	0.16	0.29	0.21	0.11	
σ_R	132.7	226.5	150.5	191.6	157.4	193.5	483.0	[km/s]
σ_ϕ	78.2	106.2	83.3	88.9	87.1	99.7	75.1	[km/s]
σ_z	63.4	73.1	78.1	181.2	152.3	185.9	241.2	[km/s]
v_{lag}^a	-11.7	24.1	-9.6	46.1	51.5	339.6	202.2	[km/s]
z_d	2.6	1.8	4.2	10.9	9.2	9.2	36.6	[kpc]
(stars) ^b								
σ_R	91.5	119.9	77.6	127.6	107.2	143.7	230.1	[km/s]
σ_ϕ	61.8	57.0	63.9	53.6	60.6	61.4	34.9	[km/s]
σ_z	39.3	35.7	41.9	138.9	104.3	196.1	88.8	[km/s]
v_{lag}	-9.8	21.3	-1.6	68.3	49.5	286.2	210.6	[km/s]
z_d	1.7	0.8	1.6	4.6	2.8	9.4	11.5	[kpc]

^aLag velocities are calculated in the frame of the local standard of rest (LSR), defined by the mean rotational speed of the primary galaxy's disk stars at the solar location; positive (negative) values indicate a slower (faster) rotation than that of the LSR.

^bFor reference, the Milky Way's thick disk is described by $(\sigma_R, \sigma_\phi, \sigma_z) = (63 \pm 6, 39 \pm 4, 39 \pm 4)$ km/s, $v_{\text{lag}} = 51.5$ km/s (Soubiran et al. 2003), and $z_d = 0.90 \pm 0.18$ kpc (Jurić et al. 2008).